

# Fermionic-bosonic couplings in a weakly-deformed odd-mass nucleus, ${}^{93}_{41}\text{Nb}$

J. N. Orce,<sup>1,2,\*</sup> J. D. Holt,<sup>2,3,4</sup> A. Linnemann,<sup>5</sup> C. J. McKay,<sup>1</sup> C. Fransen,<sup>5</sup> J. Jolie,<sup>5</sup> T.T.S. Kuo,<sup>6</sup> S. R. Leshner,<sup>1,7</sup> M. T. McEllistrem,<sup>1</sup> N. Pietralla,<sup>5,8</sup> N. Warr,<sup>5</sup> V. Werner,<sup>5,9</sup> and S. W. Yates<sup>1,10</sup>

<sup>1</sup>*Department of Physics and Astronomy, University of Kentucky, Lexington, Kentucky 40506-0055, USA*

<sup>2</sup>*TRIUMF, 4004 Wesbrook Mall, Vancouver, BC V6T 2A3, Canada*

<sup>3</sup>*Physics Division, Oak Ridge National Laboratory, P.O. Box 2008, Oak Ridge, TN 37831, USA*

<sup>4</sup>*Department of Physics and Astronomy, University of Tennessee, Knoxville, TN 37996, USA*

<sup>5</sup>*Institut für Kernphysik, Universität zu Köln, 50937 Köln, Germany*

<sup>6</sup>*Nuclear Structure Laboratory, Department of Physics and Astronomy, SUNY, Stony Brook, NY 11794-3800, USA*

<sup>7</sup>*Department of Physics, University of Wisconsin - La Crosse, 1725 State Street, La Crosse, WI 54601, USA*

<sup>8</sup>*Institut für Kernphysik, Technische Universität Darmstadt, D-64289 Darmstadt, Germany*

<sup>9</sup>*Wright Nuclear Structure Laboratory, Yale University, New Haven, CT 06520-8120, USA*

<sup>10</sup>*Department of Chemistry, University of Kentucky, Lexington, Kentucky 40506-0055, USA*

(Dated: October 29, 2018)

A comprehensive decay scheme of  ${}^{93}\text{Nb}$  below 2 MeV has been constructed from information obtained with the  ${}^{93}\text{Nb}(n,n'\gamma)$  and  ${}^{94}\text{Zr}(p,2n\gamma\gamma){}^{93}\text{Nb}$  reactions. Branching ratios, lifetimes, transition multipolarities and spin assignments have been determined. From  $M1$  and  $E2$  strengths, fermionic-bosonic excitations of isoscalar and isovector character have been identified from the weak coupling  $\pi 1g_{9/2} \otimes {}^{92}_{40}\text{Zr}$  and  $\pi 2p_{1/2}^{-1} \otimes {}^{94}_{42}\text{Mo}$  configurations. A microscopic interpretation of such excitations is attained from shell-model calculations using low-momentum effective interactions.

PACS numbers: 21.10.Re, 21.10.Tg, 25.20.Dc, 27.60.+j

## I. INTRODUCTION

Low-lying collective excitations in weakly deformed, odd-mass nuclei have rarely been studied in detail due to the structural complexity arising from the interplay of various single-particle excitations and collective degrees of freedom. With increasing angular momentum for the ground and single-particle states, bountiful excitations and a distribution of strength among several levels occurs; however, the weak coupling of a single particle to the bosonic core would provide structural simplifications. Such a scenario is present in the low-energy structure of the weakly deformed odd-mass nucleus,  ${}^{93}_{41}\text{Nb}_{52}$ , which exhibits unique, unmixed structures built on the  $\pi 1g_{9/2}$  ground state and the  $\pi 2p_{1/2}^{-1}$  proton-hole excited state.

The magnetic dipole operator,  $\hat{M}1$ , can be decomposed into an isoscalar ( $IS$ ) and an isovector ( $IV$ ) term,

$$\begin{aligned} \hat{M}1 &= IS (\Delta T = 0) + IV (\Delta T = \pm 1) \\ &\propto \sum_{i=1}^{N,Z} \mu_N \left[ \frac{1}{2} (g_{\pi}^s + g_{\nu}^s) \mathbf{s} + (g_{\pi}^l + g_{\nu}^l) \boldsymbol{\ell} \right] \\ &+ \sum_{i=1}^{N,Z} \mu_N \left[ \frac{1}{2} (g_{\pi}^s - g_{\nu}^s) \mathbf{s} + (g_{\pi}^l - g_{\nu}^l) \boldsymbol{\ell} \right] \boldsymbol{\tau}_3, \end{aligned} \quad (1)$$

where  $\boldsymbol{\ell}$ ,  $\mathbf{s}$  and  $\boldsymbol{\tau}_3$  are the orbital, spin and z-component isospin operators, respectively,  $\mu_N$  the nuclear magneton and  $g_{\pi}^l = 1\mu_N$ ,  $g_{\nu}^l = 0$  and  $g_{\pi}^s = 5.586\mu_N$ ,  $g_{\nu}^s = -3.826\mu_N$  are the orbital and spin proton and

neutron  $g$  factors in free nuclear matter, respectively. The  $IS$  term is much weaker than the  $IV$  one due to the strong cancellation of the spin  $g$  factors. Isovector excitations occur when nucleons and their spins are collectively excited. Proton and neutron spin  $g$  factors are additive in the vector part of the magnetic dipole ( $M1$ ) operator, which may lead to large  $M1$  transition strengths. The scissors mode [1] in deformed nuclei [2–5] and mixed-symmetry ( $MS$ ) states in weakly-deformed even-even nuclei [6] are examples of collective isovector excitations. The latter was predicted by the algebraic Interacting Boson Model-2 (IBM-2) with separate representations for proton and neutron bosons [7], and interpreted as a collective motion of proton and neutrons not in phase. Such isovector excitations have widely been identified in weakly-deformed even-even nuclei [6]. Both  $IS$  and  $IV$  excitations have been identified in the negative-parity structure of  ${}^{93}\text{Nb}$  built on the  $2p_{1/2}^{-1}$  proton-hole excited state [8]. Given the large quadrupole moment,  $Q_s(9/2_1^+) = -0.32(2)$ , recently determined for the ground state [9], the invocation of a simpler vibrational picture seems unnecessary, and this work provides a microscopic many-body interpretation of such isovector excitations.

In fact,  $MS$  states have been explained from a shell-model ( $SM$ ) basis by Lisetskiy and collaborators [10] using a surface delta interaction with tuned parameters. Large isoscalar  $E2$  matrix elements were found between states with  $MS$  assignments and interpreted as excitations with similar  $pn$  symmetry. In a microscopic many-body framework, shell-model calculations using a  ${}^{88}\text{Sr}$  core and effective low-momentum interactions  $V_{\text{low } k}$  [11] have successfully accounted for excitation energies, level densities,  $M1$  and  $E2$  transition strengths, isoscalar and

\* jnorce@triumf.ca; <http://www.pa.uky.edu/~jnorce>

isovector excitations, and both spin and orbital contributions to the  $M1$  transition matrix elements in the negative-parity structure of  $^{93}\text{Nb}$  [8]. As a successor to that work, we present a more extensive spectroscopic and microscopic study of  $^{93}\text{Nb}$ , including both positive- and negative-parity structures.

## II. EXPERIMENTAL DETAILS

The nucleus  $^{93}\text{Nb}$  has been studied with the  $(n,n'\gamma)$  reaction at the University of Kentucky and in a  $^{94}\text{Zr}(p,2n)^{93}\text{Nb}$   $\gamma$ - $\gamma$  coincidence experiment at the University of Cologne.

### A. $^{93}\text{Nb}(n,n'\gamma)$ experiments

Excitation functions, lifetimes and branching ratios were measured using the  $^{93}\text{Nb}(n,n'\gamma)$  reaction [12] at neutron energies ranging from 1.5 to 2.6 MeV. Neutrons were provided by the 7-MV electrostatic accelerator at the University of Kentucky through the  $^3\text{H}(p,n)^3\text{He}$  reaction. The scattering sample was 56 g of Nb, which is naturally monoisotopic, in a  $3\times 2$  cm cylinder. Pulsed-beam techniques were used to reduce background, with beam pulses separated by 533 ns and bunched to about 1 ns. The time-of-flight technique for background suppression was employed by gating on the appropriate prompt time windows [12]. Finally,  $\gamma$  rays were detected using a BGO Compton-suppressed 55% HPGe spectrometer with 2.0 keV resolution. Both excitation functions and angular distributions were normalized to the neutron flux.

From the angular distribution experiments, lifetimes were determined through the Doppler-shift attenuation method following the  $(n,n'\gamma)$  reaction [13]. Here, the shifted  $\gamma$ -ray energy is given by,

$$E_\gamma(\theta_\gamma) = E_{\gamma_0} \left[ 1 + \frac{v_0}{c} F(\tau) \cos\theta_\gamma \right], \quad (2)$$

with  $E_{\gamma_0}$  being the unshifted  $\gamma$ -ray energy,  $v_0$  the initial recoil velocity in the center of mass frame,  $\theta$  the angle of observation and  $F(\tau)$  the attenuation factor, which is related to the nuclear stopping process described by Blaugrund [14]. Finally, the lifetimes of the states can be determined by comparison with the  $F(\tau)$  values calculated using the Winterbon formalism [15].

Furthermore,  $\gamma$ -ray coincidences were observed through the  $(n,n'\gamma\gamma)$  reaction at a neutron energy of 3 MeV in order to identify the decay paths of  $\gamma$  rays, measure their branching ratios, and confirm the results from the excitation functions. The coincidence methods have been described by McGrath *et al.* [16].

### B. $^{94}\text{Zr}(p,2n)^{93}\text{Nb}$ angular correlation experiment

For odd-mass nuclei, particularly those with high ground-state spins, the angular distributions of the photons from scattering reactions are rather isotropic, and

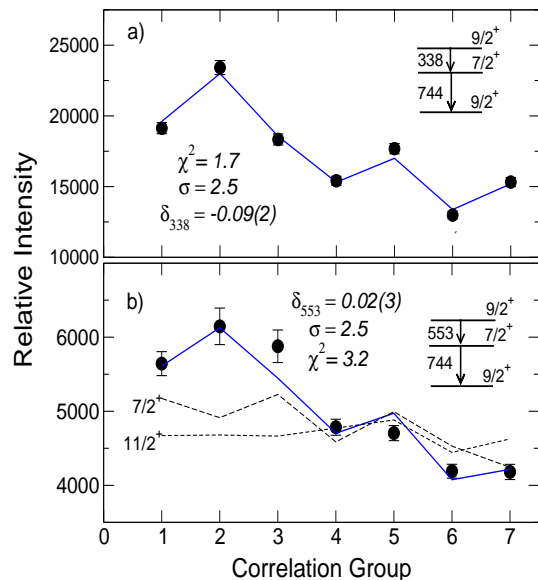


FIG. 1. (Color online) Angular correlation plots for a) the 338-keV and b) the 553-keV transitions gated by the 744 keV  $\gamma$  ray. The fits to the data give mixing ratios of  $\delta_{338} = -0.09(2)$  (in agreement with previous work,  $\delta_{338} = -0.12(5)$ ) and a more precise  $\delta_{553} = 0.02(3)$  as compared with previous work,  $\delta = -0.3_{-7}^{+3}$  [23]. Dashed lines indicate other angular correlation fits with unlikely spins for the 1297.4 keV level. The fitting parameter  $\sigma$  is the width of the magnetic substate distribution, usually found to be between 2 and 3.

the  $(n,n'\gamma)$  data cannot be used generally for assigning the spins of excited states. Complementarily, from a  $\gamma$ - $\gamma$  coincidence experiment with the  $^{94}\text{Zr}(p,2n\gamma\gamma)^{93}\text{Nb}$  reaction, many multipolarities and spin assignments could be determined, and branching ratios were measured. The proton beam provided by the 10-MV tandem accelerator at the University of Cologne bombarded a 2 mg/cm<sup>2</sup> thick  $^{94}\text{Zr}$  target enriched to 96.93% with beam currents from 2 to 3  $\mu\text{A}$ . The proton energies were in the range of 11.5 to 19 MeV. The de-exciting  $\gamma$  rays were detected using the HORUS spectrometer [17], comprised of 16 HPGe detectors with the following features: a) seven of the detectors formed a EUROBALL cluster detector [18] with the central detector placed at  $\theta=90^\circ$  with respect to the beam axis and  $\phi=0^\circ$ , where  $\phi$  is the clockwise angle around the beam axis; b) four detectors placed at  $\theta=45^\circ$  and  $135^\circ$  in a vertical plane above and below the beam axis were complemented by Compton suppression shields; c) the remaining detectors were placed in the  $\theta=90^\circ$  plane and at angles of  $\phi=55^\circ$ ,  $125^\circ$ ,  $235^\circ$  and  $305^\circ$ . When possible, we determined the  $E2/M1$  mixing ratio,  $\delta^2 = \Gamma_{f,E2}/\Gamma_{f,M1}$  [19], by fitting the angular correlation data as a function of the angles,  $\theta_1$ ,  $\theta_2$  and  $\phi$ , following the formalism developed by Krane and Steffen [20]. The current results are in agreement with the most intense transitions identified in previous work [21, 22]. As an example of this agreement, the top panel of Fig.

1 shows an angular correlation plot for the previously known 338-keV  $\gamma$  ray depopulating the 1082-keV one-phonon excitation. A value of  $\delta_{744} = 0.26(8)$  was fixed from the angular correlation analysis of  $\gamma$  rays populating the 744-keV level.

### III. DATA ANALYSIS AND RESULTS

In previous work by van Heerden and McMurray [21], angular momenta, parities and transition rates for several of the first ten states (up to 1.1 MeV) were presented. The low-lying structure of  $^{93}\text{Nb}$  is dominated by the  $\pi 1g_{9/2}$  and  $\pi 2p_{1/2}^{-1}$  single-particle and proton-hole excitations, respectively, and  $jj$  couplings built on these [21, 22, 24–26]. In particular, the  $\pi 1g_{9/2}$  ground state couples to the  $2_1^+$  state of the  $^{92}\text{Zr}$  core to give a quintet of isoscalar excitations,  $J^\pi = 5/2^+, 7/2^+, 9/2^+, 11/2^+$  and  $13/2^+$ . The  $3/2^-$  and  $5/2^-$  states are also identified as being built on the low-lying  $\pi 2p_{1/2}^{-1}$  excitation. Our results are in agreement with previous work.

Excitation functions, together with the analysis of gated coincidence spectra, allowed the construction of a comprehensive level scheme up to 2.2 MeV. Figure 2 shows the total projection of the coincidence matrix built from the  $^{93}\text{Nb}(n,n'\gamma\gamma)$  experiment, with the main  $\gamma$ -ray transitions depopulating the nucleus labeled. The data also support two well-defined and nearly separate structures as the main characteristic of this nucleus. Figure 3 shows typical background-subtracted spectra gated on the 744-keV and 780-keV transitions feeding the ground state and  $1/2^-$  state, respectively, indicating the different decay patterns as well as the quality of the data. These two separate structures are presented and discussed according to the parity of the states and their *IS/IV* character.

#### A. Particle-core (*PC*) weak coupling model

The states of an odd-*A* nucleus can be described in terms of a valence nucleon coupled to the excited states of the neighboring even-even core [27–29]. In the weak-coupling limit, the coupling Hamiltonian can be treated as a perturbation, whereas the intermediate coupling also allows for mixing between several single-particle states coupled to core excitations. The angular momentum of the core,  $J_{core}$  and single-particle (or particle-hole) states,  $J_{sp}$ , couple to form a multiplet of states with a total angular momentum [21, 30–33] given by,

$$|J_{sp} - J_{core}| \leq J_{core} \otimes J_{sp} \leq |J_{sp} + J_{core}|. \quad (3)$$

In fact, low-lying excited states in  $^{93}\text{Nb}$  can be regarded as resulting from the coupling of a  $1g_{9/2}$  proton to a  $^{92}\text{Zr}$  core and a  $2p_{1/2}^{-1}$  proton-hole to a  $^{94}\text{Mo}$  core [21]. These couplings result in two independent and unmixed one-phonon structures of opposite parity: a) a quintet of

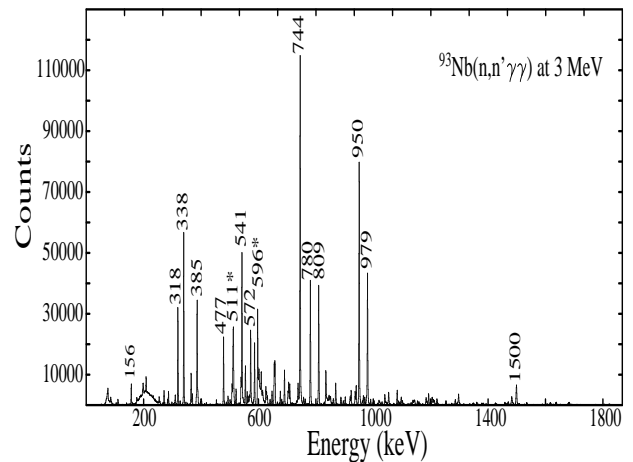


FIG. 2. Background-subtracted total projection of the  $\gamma$ - $\gamma$  coincidence matrix from the  $^{93}\text{Nb}(n,n'\gamma\gamma)$  reaction at an incident neutron energy of 3 MeV. The labelled transitions belong to  $^{93}\text{Nb}$ , except for those indicated by asterisks (electron-positron annihilation and radiation produced by neutrons striking the HPGe detectors.)

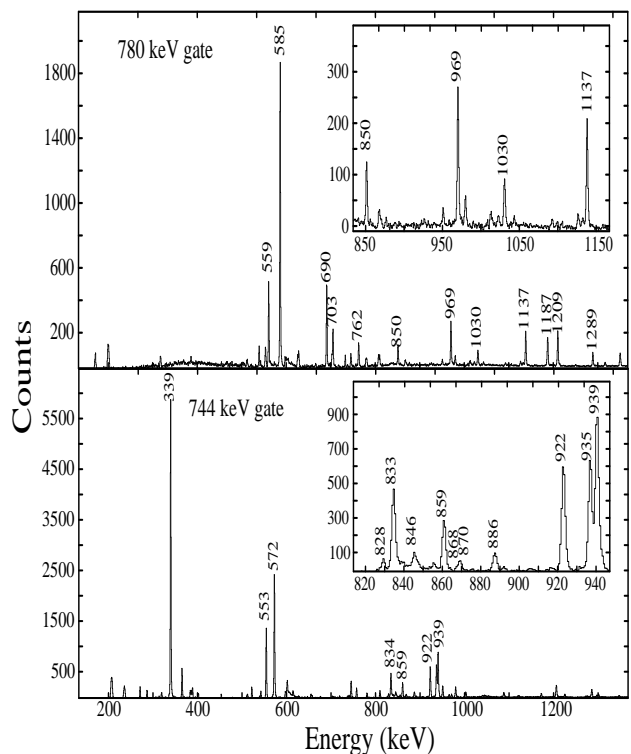


FIG. 3. Background-subtracted  $\gamma$ -ray spectra gated by the 744- and the 780-keV transitions in the  $^{93}\text{Nb}(n,n'\gamma\gamma)$  coincidence matrix.

positive-parity states built on the  $J^\pi=9/2^+$  ground state, resulting from the  $\pi 1g_{9/2} \otimes (2_1^+, ^{92}\text{Zr})$  *PC* coupling; and b) a pair of negative-parity states built on the isomeric (with a half-life of 16 years)  $J^\pi=1/2^-$  state at 31 keV, which corresponds to the  $\pi 2p_{1/2}^{-1} \otimes (2_1^+, ^{94}\text{Mo})$  configuration.

TABLE I. Properties of low-lying positive-parity states in  $^{93}\text{Nb}$  below 2.2 MeV. Excitation energies, spins, lifetimes,  $\gamma$ -ray energies, branching and mixing ratios, initial and final spins of the states, and reduced transition probabilities are listed. An asterisk labels newly identified levels and  $\gamma$ -ray transitions. Uncertainties in the energies are 0.2 keV.

$E_{level}$ (keV)	$\tau$ (fs)	$J_i^\pi \rightarrow J_f^\pi$	$E_\gamma$ (keV)	$I_\gamma$	$\delta$	$B(M1)$ ( $\mu_N^2$ )	$B(E2)$ (W.u.)	$B(M1)$ [Shell Model]	$B(E2)$
0.0	stable								
744.0		7/2 <sup>+</sup> 9/2 <sup>+</sup>	744.0	100	0.28(8)			0.09591	7.836
809.1		5/2 <sup>+</sup> 7/2 <sup>+</sup> 9/2 <sup>+</sup>	65.0 808.6	<1 100(2)	(M1/E2) E2			0.1023 -	3.80 11.313
949.8		13/2 <sup>+</sup> 9/2 <sup>+</sup>	949.8	100	E2			-	8.050
979.6	715 <sup>+350</sup> <sub>-180</sub>	11/2 <sup>+</sup> 9/2 <sup>+</sup>	978.8	100	-0.13(7)			0.04328	5.761
1082.6	>1245	9/2 <sup>+</sup> 11/2 <sup>+</sup> 7/2 <sup>+</sup> 9/2 <sup>+</sup>	103.7* 338.6 1082.6	3(2) 100(2) 38(2)	M1/E2 M1/E2 M1/E2			1.747 0.1795 0.00731	1.091 2.299 3.992
1127.0 <sup>IS</sup>		7/2 <sup>+</sup> 5/2 <sup>+</sup>	318.3	100(2)	-0.20(6)			0.016	0.6033
1297.4 <sup>IV</sup>	380 <sup>+110</sup> <sub>-75</sub>	9/2 <sup>+</sup> 11/2 <sup>+</sup> 7/2 <sup>+</sup> 9/2 <sup>+</sup>	318.3 553.1 1297.4	31(5) 61(5) 100(5)	(M1/E2) -0.03(5) 0.31(9)	<0.9 0.33(5) 0.04(1)	0.6(1) 1.2(2)	0.02185 0.2476 0.00366	1.420 2.299 0.0591
1315.7 <sup>IV</sup>	530 <sup>+450</sup> <sub>-170</sub>	5/2 <sup>+</sup> 5/2 <sup>+</sup> 7/2 <sup>+</sup>	506.7 571.5	24(4) 100(4)	-1.4(8) 0.14(4)	0.05(4) 0.45(25)	235 <sup>+300</sup> <sub>-200</sub> 15(10)	0.190 0.4072	0.3816 3.864
1334.9 <sup>IS</sup>		17/2 <sup>+</sup> 13/2 <sup>+</sup>	385.1	100(2)	E2				
1483.6 <sup>IV</sup>	65(5)	7/2 <sup>+</sup> 9/2 <sup>+</sup> 5/2 <sup>+</sup> 9/2 <sup>+</sup>	400.8* 674.8 1483.8	7(2) 27(2) 100(2)	(M1/E2) -0.11(8) -0.13(7)	<0.7 0.58(6) 0.20(2)	9(1) 0.9(6)	0.3459 0.1970 0.00422	0.02121 0.1264 5.568
1490.9 <sup>IS</sup>	>750	15/2 <sup>+</sup> 17/2 <sup>+</sup> 13/2 <sup>+</sup>	156.0 541.1	14(2) 100(2)	(M1/E2) -0.11(2)	<0.04 <0.47	<12		
1603.5 <sup>IS</sup>	465 <sup>+250</sup> <sub>-125</sub>	11/2 <sup>+</sup> 9/2 <sup>+</sup> 11/2 <sup>+</sup> 13/2 <sup>+</sup> 7/2 <sup>+</sup> 9/2 <sup>+</sup>	520.9 624.4 653.6 859.5 1603.5	13(3) 32(3) 100(3) 22(3) 23(3)	-0.07(9) 0.11(6) 0.17(3) - (M1/E2)	0.05(3) 0.08(3) 0.22(9) - <0.1	0.6(4) 1.5(6) 8(3) 17(7) <1	0.03669 0.05017 0.1282 - 0.00566	1.505 0.6245 0.6027 2.817 0.05378
1665.6 <sup>IS</sup>	350 <sup>+100</sup> <sub>-65</sub>	5/2 <sup>+</sup> 5/2 <sup>+</sup> 7/2 <sup>+</sup> 9/2 <sup>+</sup>	856.9 921.6 1665.7*	<1 100(2) 2(2)	(M1/E2) 1.4(2) E2	<0.01 0.07(2) -	90(35) <1	0.1079 0.0740 -	0.3015 2.891 3.771
1679.8 <sup>IS</sup>	315 <sup>+85</sup> <sub>-60</sub>	7/2 <sup>+</sup> 5/2 <sup>+</sup> 9/2 <sup>+</sup> 5/2 <sup>+</sup> 7/2 <sup>+</sup> 9/2 <sup>+</sup>	364.1 382.4 870.1* 935.7 1679.7	60(3) 16(3) 7(3) 100(3) 36(3)	-0.17(9) (M1/E2) (M1/E2) 0.09(9) (M1/E2)	1.0(2) <0.25 <0.01 0.10(2) <0.01	130(50) 0.5(1)	0.00460 0.00001 0.00650 0.00023 0.00244	1.204 1.150 1.995 2.452 0.4702
1683.3	150 <sup>+25</sup> <sub>-20</sub>	9/2 <sup>+</sup> 9/2 <sup>+</sup> 11/2 <sup>+</sup> 7/2 <sup>+</sup> 9/2 <sup>+</sup>	600.7* 704.2 939.3 1683.2	17(4) 42(4) 100(4) 54(4)	(M1/E2) 0.21(4) -0.20(4) -0.34(25)	<0.15 0.20(4) 0.21(3) 0.02(1)	10(2) 5.4(8) 1(1)	0.0117 0.05473 0.0962 0.00496	0.01288 0.04624 0.6608 0.2582
1686.3	250 <sup>+60</sup> <sub>-40</sub>	13/2 <sup>+</sup> 11/2 <sup>+</sup> 13/2 <sup>+</sup> 9/2 <sup>+</sup>	707.4* 736.5 1686.3	88(4) 90(4) 100(4)	-0.09(3) -0.27(13) E2	0.20(5) 0.17(4) -	1.9(4) 13(3) 3(1)	0.01221 0.04217 -	1.480 0.06688 0.1624
1703.5 <sup>IS</sup>	220 <sup>+280</sup> <sub>-90</sub>	3/2 <sup>+</sup> 5/2 <sup>+</sup> 5/2 <sup>+</sup>	387.9* 894.8*	100(4) 87(4)	-0.02(6) -0.3(1)	2.4(2.0) 0.15(12)	4(3) 10(6)	0.02740 0.5956	4.030 5.015

$E_{level}$ (keV)	$\tau$ (fs)	$J_i^\pi \rightarrow J_f^\pi$	$E_\gamma$ (keV)	$I_\gamma$	$\delta$	$B(M1)$ ( $\mu_N^2$ )	$B(E2)$ (W.u.)	$B(M1)$ [Shell Model]	$B(E2)$	IS	IV
1773.1 <sup>IS</sup>	125 <sup>+20</sup> <sub>-15</sub>	(1/2 <sup>+</sup> )	(5/2 <sup>+</sup> ) 5/2 <sup>+</sup>	646.0* 964.0	86(4) 100(4)	E2 E2		- -	12.36 5.126		
1812.2	150 <sup>+50</sup> <sub>-35</sub>		(17/2 <sup>+</sup> )	477.3	100						
1910.6 <sup>IV</sup>	200 <sup>+40</sup> <sub>-30</sub>	11/2 <sup>+</sup>	9/2 <sup>+</sup> 9/2 <sup>+</sup> 9/2 <sup>+</sup>	613.4* 828.1* 1910.6	10(6) 7(6) 100(6)	-0.20(12) -0.61(17) (M1/E2)	0.08(3) 0.02(1) <0.03	5(2) 6(3) 0.00032	0.1171 3.748 2.444		
1916.1 <sup>IV</sup>	90(10)	7/2 <sup>+</sup>	5/2 <sup>+</sup> 9/2 <sup>+</sup> 5/2 <sup>+</sup> 7/2 <sup>+</sup> 9/2 <sup>+</sup>	600.4* 833.4 1107.2* 1172.1* 1915.5*	36(4) 100(4) 4(4) 12(4) 5(4)	0.06(4) -0.01(2) (M1/E2) (M1/E2) (M1/E2)	0.66(10) 0.69(10) <0.01 <0.03 <0.01	4(1) 0.1(1)			
1949.6 <sup>IS</sup>	770 <sup>+1650</sup> <sub>-320</sub>	7/2 <sup>+</sup>	(5/2 <sup>+</sup> ) 9/2 <sup>+</sup> 11/2 <sup>+</sup> 5/2 <sup>+</sup> 7/2 <sup>+</sup>	270.1* 866.8* 971.1* 1140.8 1205.9	100(5) 9(5) 100(5) 92(5)	M1/E2 M1/E2 0.21(5) M1/E2					
1949.7*	925 <sup>+3700</sup> <sub>-425</sub>	(7/2 <sup>+</sup> )	(9/2 <sup>+</sup> ) 11/2 <sup>+</sup> 9/2 <sup>+</sup>	266.4* 346.4* 1949.8	26(4) 41(4) 82(4)	(M1/E2) E2 (M1/E2)					
1968.3		(11/2 <sup>+</sup> , 13/2 <sup>+</sup> )	11/2 <sup>+</sup> 15/2 <sup>+</sup>	365.0* 477.3	45(3) 100(3)	(M1/E2) (M1/E2)					
1968.8 <sup>IS</sup>	160 <sup>+35</sup> <sub>-30</sub>	11/2 <sup>+</sup>	13/2 <sup>+</sup> 9/2 <sup>+</sup> 11/2 <sup>+</sup> 13/2 <sup>+</sup> 7/2 <sup>+</sup> 9/2 <sup>+</sup>	282.5 285.6 990.0 1019.0 1225.0* 1968.9	27(5) 34(5) 64(5) 38(5) 12(5) 100(5)	(M1/E2) (M1/E2) -0.83(16) -0.28(7) E2 (M1/E2)	<1.5 <1.8 0.05(2) 0.04(1) <0.2	20(7) 2(1) 3(2)			
2002.5 <sup>IS</sup>	> 800	11/2 <sup>+</sup>	11/2 <sup>+</sup> 7/2 <sup>+</sup> 15/2 <sup>+</sup> 11/2 <sup>+</sup> 13/2 <sup>+</sup>	399.1* 502.4* 511.5* 1023.7* 1052.8	20(2) 12(2) 10(2) 100(2)	(M1/E2) E2 E2 M1/E2 -0.63(7)					
2122.6*, <sup>IS</sup>	115 <sup>+30</sup> <sub>-20</sub>	9/2 <sup>+</sup>	7/2 <sup>+</sup> 11/2 <sup>+</sup> 7/2 <sup>+</sup> 9/2 <sup>+</sup>	639.0* 1143.7* 1378.9* 2122.6*	36(3) 71(3) 29(3) 100(3)	(M1/E2) 3.8 <sup>+1.9</sup> <sub>-1.0</sub> -1.9(8) (M1/E2)	<0.2 0.01(1) 0.02(1) <0.02	0.09535 29(6) 0.2(2) 0.00078	0.0023 2.275 0.1651 1.508		
2162.6 <sup>IS</sup>	410 <sup>+300</sup> <sub>-125</sub>	(13/2 <sup>+</sup> )	15/2 <sup>+</sup> 11/2 <sup>+</sup> 13/2 <sup>+</sup>	671.7* 1183.7 1212.8*	25(4) 100(4) 61(4)	(M1/E2) (M1/E2) (M1/E2)					
2170.4 <sup>IS</sup>	350 <sup>+165</sup> <sub>-90</sub>	9/2 <sup>+</sup>	9/2 <sup>+</sup> 11/2 <sup>+</sup> 13/2 <sup>+</sup> 5/2 <sup>+</sup> 7/2 <sup>+</sup>	1087.6* 1192.5 1221.6 1361.1* 1426.1*	10(3) 100(3) 60(3) 31(3) 27(3)	(M1/E2) (M1/E2) E2 E2 (M1/E2)					
2184.0*	110 <sup>+45</sup> <sub>-30</sub>	(13/2 <sup>+</sup> )	(17/2 <sup>+</sup> ) (9/2 <sup>+</sup> )	849.1* 480.5*	100(2) <2	E2 E2					

### B. $\pi 1g_{9/2} \otimes (2_1^+, {}^{92}\text{Zr})$ configuration

The  $\pi 1g_{9/2} \otimes (2_1^+, {}^{92}\text{Zr})$  configuration assignment is supported by the center-of-gravity theorem [21, 30], which implies, through the j-j coupling shell model, the exist-

tence of geometrical relations among the spectra of neighboring nuclei. The center-of-gravity energy of the one-phonon system,  $\Delta E_{CG}$ , is then given by the relation,

$$(2j_p + 1)\Delta E_{CG} = (2J_{core} + 1)^{-1} \sum_{J_3} (2J_3 + 1)E_{J_3} \quad (4)$$

where  $j_p$  is the angular momentum of the coupled particle (in our case  $g_{9/2}$ ),  $J_{core}$  is the angular momentum of the core state ( $2^+$ ), and  $J_3$ ,  $E_{J_3}$  are the spins and excitation energies, respectively, of the single one-phonon states. Considering the first 5 excited positive-parity states in  $^{93}\text{Nb}$  as one-phonon excitations and  $Z=40$  as a semi-closed shell for protons, the predicted center-of-gravity excitation energy is 934 keV. This energy is in striking agreement with the 934.5 keV measured for the first excited  $2^+$  state in  $^{92}\text{Zr}$  [34, 35]. In addition, from Coulomb excitation studies, the sum of  $B(E2)\uparrow$  values for the quintet of one-phonon states proposed in  $^{93}\text{Nb}$ ,  $765(11) \text{ e}^2 \text{ fm}^4$  (weighted average from Refs. [22, 36–38]), matches well the excitation of the  $2^+$  core state,  $795(56) \text{ e}^2 \text{ fm}^4$  (weighted average from Refs. [36, 39]), in  $^{92}\text{Zr}$ . Again, these data support the weak-coupling nature of these states [37, 39].

However, the above arguments are not consistent with the results from Kent *et al.* in the positive-parity structure, where inelastic proton scattering studies through isobaric analog resonances in  $^{94}\text{Mo}$  did not support the weak coupling in  $^{93}\text{Nb}$  [40]. The proposed  $9/2_2^+$  member of the quintet at 1082.6 keV decays preferentially to the  $7/2_1^+$  state at 744.0 keV rather than by a 1082.6 keV transition to the ground-state; which breaks the selection rule between vibrational states ( $\Delta n_\lambda = \pm 1$ ). Two-state mixing calculations between the 1082.6-keV and ground states were done in an attempt to explain this anomalous decay [37], and the results are in agreement with decay strengths in neighboring  $^{92}\text{Mo}$  and  $^{94}\text{Mo}$  nuclei.

### C. $\pi 2p_{1/2}^{-1} \otimes (2_1^+, ^{94}\text{Mo})$ configuration

Low-lying negative-parity states in  $^{93}\text{Nb}$  can be regarded as resulting from the  $\pi 2p_{1/2}^{-1} \otimes (2_1^+, ^{94}\text{Mo})$  coupling. A doublet of negative-parity states ( $J^\pi=3/2^-$  at 687.4 keV and  $J^\pi=5/2^-$  at 810.7 keV) built on the  $J^\pi=1/2_1^-$  state confirms this assignment. Recently, we have studied excited states built on this doublet and identified isovector excitations that correspond to the  $2_{1,IV}^+$  states found in neighboring even-even nuclei [8]. Identifications are based on  $M1$  and  $E2$  strengths, energy systematics, and spin-parity assignments and from the comparison with  $SM$  calculations with the low-momentum nucleon-nucleon interaction,  $V_{low-k}$  [11]. Similar investigations will be provided in this work for the  $IS$  negative-parity excitations, where seven states are expected from the  $PC$  model, i.e., in addition to the  $1/2_1^-$  state for the single-particle state,  $3/2^-$  and  $5/2^-$  states for the one-phonon excitations, and  $3/2^-$ ,  $5/2^-$ ,  $7/2^-$ , and  $9/2^-$  states for the two-phonon excitations.

### D. Positive-parity states

Five new levels and 40 additional  $\gamma$ -ray transitions have been identified in this work. Table I lists the positive-parity states below 2.2 MeV, together with the  $\gamma$  rays depopulating them. The decay properties evince a complex structure of levels decaying to either the ground state or lowest  $IS$  excitations. Despite possible admixtures of  $IS$  and  $IV$  wavefunctions in the odd-mass case, corresponding  $MS$  decay signatures might be expected analogous to those observed in the even- $A$   $N = 52$  isotones [41, 42]. From strong  $M1$  transitions to the  $IS$  states and weakly collective  $E2$  transitions to the ground state, we propose three candidates for  $IV$  excitations, the  $9/2_2^+$ ,  $5/2_2^+$  and  $7/2_3^+$  levels at 1297.4, 1315.7 and 1483.6 keV, respectively. We propose them to be members of the quintet of  $IV$  excitations ( $5/2_{IV}^+$ ,  $7/2_{IV}^+$ ,  $9/2_{IV}^+$ ,  $11/2_{IV}^+$  and  $13/2_{IV}^+$ ) arising from the  $\pi 1g_{9/2} \otimes (2_{1,IV}^+, ^{92}\text{Zr})$  coupling. Furthermore, from enhanced  $B(E2)$  values to the  $9/2_{IV}^+$  state, we tentatively propose the  $11/2^+$  level at 1910.6 keV as a fragment of the scissors mode. Additional details are provided below. Further assignments in Table I are tentative due to the complex structure and possibility of intermediate coupling.

#### 1. 1297.4 keV $9/2_{IV}^+$ state

The 1297.4 keV level has been firmly assigned as  $J^\pi=9/2^+$  from the analysis of the angular correlation of the decay branches (see Table I and the bottom panel of Fig. 1). A mean lifetime of  $380_{-75}^{+110}$  fs has been determined for this level from the Doppler-shift attenuation data. This value is in agreement with, but more accurate than the  $300_{-100}^{+300}$  fs lifetime measured in previous work [43]. Hence, the 553.1 and 318.3 keV transitions have large  $B(M1)$  values of  $0.33(5)$  and  $<0.9 \mu_N^2$ , respectively. This level also decays by a small  $E2$  strength to the ground state,  $B(E2; 9/2_{IV}^+ \rightarrow 9/2_1^+) = 1.3(3) \text{ W.u.}$  Both features are typical signatures for  $MS$  states.

#### 2. 1315.7 keV $5/2_{IV}^+$ state

A  $J^\pi=5/2^+$  assignment has been given to this level from the angular correlation of the decay branches (see Table I) together with a mean lifetime of  $530_{-170}^{+450}$  fs from the Doppler-shift attenuation data. The 571.5-keV transition to the  $7/2_1^+$  has a large  $B(M1)$  value of  $0.45(25) \mu_N^2$ ; nonetheless, the 506.7-keV transition to the  $5/2_1^+$  state presents a large  $B(E2)$  value. Hence, the excitation has not a pure  $IV$  character and intermediate coupling may mix  $IS$  and  $IV$  states.

### 3. 1483.6 keV $7/2_{IV}^+$ state

The 1483.6 keV level was previously assigned as  $J^\pi=(7/2^+, 9/2^+)$ . The angular correlation analysis of the branches depopulating this state (see Table I) has firmly assigned it as  $J^\pi=7/2^+$ . A short mean lifetime of 65(5) fs has been determined for the first time. The 674.8- and 400.8-keV transitions have large  $B(M1)$  values of 0.58(6) and  $<0.7 \mu_N^2$ , respectively. The level decays to the ground state through a weakly collective E2 transition,  $B(E2) = 0.9(6)$  W.u. Again, we find the characteristic features of a *MS* state.

### 4. 1910.6 keV $11/2^+$ state

The 1910.6 keV level has been assigned as  $J^\pi=11/2^+$ , in disagreement with previous work, where  $J^\pi=7/2^{(+)}$  was proposed [44]. A lifetime of  $200_{-30}^{+40}$  fs has been determined for this level, which decays with a weakly collective  $B(E2)$  value of 5(2) W.u. to the proposed 1297.4 keV *IV* excitation. From this  $B(E2)$  value and the spin assignment of the state, we tentatively propose the 1910.6 keV level as a fragment of a second-order *IV* excitation identified in the even-even neighbors. Arguments against this assignment are that neither the 1910.6 keV transition to the ground state nor the 828.1-keV  $\gamma$  ray to the  $9/2_2^+$  state have the enhanced  $B(M1)$  character expected for an *IV* excitation, and the scissors mode is generally identified at about 3 MeV. Nevertheless, the *IV* assignment is plausible since large fragmentation of the scissors mode strength has been observed in the 2 to 4 MeV energy range in systematic studies of odd-A rare earth nuclei [3, 4, 45].

### 5. 1968.8 keV $11/2_{IS}^+$ state

Although the spin was assigned as  $J^\pi=11/2^+$  and we have a newly determined lifetime of  $160_{-30}^{+35}$  fs for this state, only upper values for the *M1* strengths of some of the transitions could be determined. The large  $B(E2) = 20(7)$  W.u. observed for the 990.0-keV transition to the  $11/2_1^+$  *IS* excitation is noteworthy.

### 6. 2122.6 keV $9/2_{IS}^+$ state

With an assigned  $J^\pi=9/2^+$  and a lifetime of  $115_{-20}^{+30}$  fs, this state presents small  $B(M1)$  values ( $<0.2 \mu_N^2$ ) and a relatively large  $B(E2) = 29(6)$  W.u. to the  $11/2_1^+$  isoscalar excitation.

## E. Negative-parity states

Although some relevant information concerning the negative-parity states in  $^{93}\text{Nb}$  has already been pub-

lished [8], we present additional data collected in our measurements. Table II lists the results for levels up to 2.1 MeV.

### 1. 1284.8 $5/2^-$ state

The 1284.8 keV level has been assigned as  $J^\pi=5/2^-$ . A lifetime of  $250_{-50}^{+80}$  fs has been measured for this level, which decays through a large  $B(E2)$  value of  $32_{-9}^{+10}$  W.u. to the  $1/2^-$  single-particle state, indicating a strong correlation between the wavefunctions of these states.

### 2. 1370.1 $5/2_{IS}^-$ state

The 1370.1 keV level has been assigned as  $J^\pi = 5/2^-$ . A lower limit for the lifetime of  $>790$  fs has been determined for this level, giving upper limits for the  $B(E2)$  values to the  $3/2_1^-$  and  $5/2_1^-$  one-phonon states of  $<7$  and  $<54$  W.u., respectively. No decay to the ground state has been observed, supporting its *IS* character.

### 3. 1395.8 $7/2_{IS}^-$ state

The 1395.8 keV level has been assigned as  $J^\pi = 7/2^-$ . A lower limit for the lifetime of  $>790$  fs has been determined for this level, giving upper limits for the  $B(E2)$  values to the  $3/2_1^-$  and  $5/2_1^-$  states of  $<18$  and  $<5$  W.u., respectively. No decay to the ground state has been observed, supporting its *IS* character. In addition, the strong isoscalar character of the transitions to the one-phonon states, listed in the last two columns of Table II, supports its *IS* assignment.

### 4. 1500.0 keV $9/2_{IS}^-$ state

This state was previously assigned as  $J^\pi = 7/2^{(-)}$  [44]. Nevertheless, a  $J^\pi = 9/2^-$  assignment is a better solution from the angular correlation fits. It also presents the longest lifetime, a newly measured 1170(300) fs, with respect to the other levels discussed in this section. An enhanced  $B(E2)$  value of  $27_{-9}^{+15}$  W.u. for the 689.6 keV E2 transition to the  $5/2^-$  one-phonon state suggests this state as a member of the negative-parity *IS* coupling excitations. This large  $B(E2)$  value is also predicted by our *SM* calculations, together with the isoscalar character of the transition to the one-phonon states.

### 5. 1572.1 $3/2_{IS}^-$ state

A lifetime of  $280_{-100}^{+210}$  fs has been determined for this level, giving large  $B(E2)$  values to the  $3/2^-$  and  $5/2^-$  one-phonon states of  $36_{-19}^{+27}$  and  $21_{-10}^{+12}$  W.u., respectively.

TABLE II. Properties of low-lying negative-parity states in  $^{93}\text{Nb}$  up to 2.1 MeV. Level and  $\gamma$ -ray energies, branching and mixing ratios, initial and final spin of the states, lifetimes, and reduced transition probabilities are listed. An asterisk labels newly identified levels and  $\gamma$  ray transitions. Shell model  $B(M1)$  and  $B(E2)$  predictions for relevant transitions are shown on the right with the isoscalar (IS) and isovector (IV) components of the  $E2$  operator. Uncertainties in the energies are 0.2 keV.

$E_L$ (keV)	$\tau$ (fs)	$J_i^- \rightarrow J_f^-$	$E_\gamma$ (keV)	$I_\gamma$	$\delta$	$B(M1)$ ( $\mu_N^2$ )	$B(E2)$ (W.u.)	$B(M1)$ $B(E2)$ [Shell Model]	IS	IV
30.9		$\frac{1}{2}^- \rightarrow \frac{9}{2}^+$			$M4$					
687.4	$400_{-20}^{+70q}$	$\frac{3}{2}^- \rightarrow \frac{1}{2}^-$	655.9	100	(M1/E2)					
810.7		$\frac{5}{2}^- \rightarrow \frac{1}{2}^-$	799.6	100	E2					
		$\frac{3}{2}^- \rightarrow \frac{3}{2}^-$	123.3*	< 1	(M1/E2)					
1284.8	$250_{-50}^{+80}$	$\frac{5}{2}^- \rightarrow \frac{1}{2}^-$	1253.5	100(4)	$E2$		$32_{-9}^{+10}$	-	-	-
		$\frac{3}{2}^- \rightarrow \frac{3}{2}^-$	597.3*	25(4)	0.14(4)	$0.20_{-0.08}^{+0.10}$	$6_{-2}^{+3}$	-	-	-
		$\frac{5}{2}^- \rightarrow \frac{5}{2}^-$	473.9*	5(4)	(M1)	<0.08		-	-	-
1370.1 <sup>IS</sup>	> 790	$\frac{5}{2}^- \rightarrow \frac{3}{2}^-$	683.2*	30(4)	-0.34(5)	<0.05	<7	-	-	-
		$\frac{5}{2}^- \rightarrow \frac{5}{2}^-$	559.4	100(4)	-0.32(7)	<0.29	<54	-	-	-
1395.8 <sup>IS</sup>	> 790	$\frac{7}{2}^- \rightarrow \frac{3}{2}^-$	708.6	9(4)	$E2$		<18	-	8.50	28.61 -13.85
		$\frac{5}{2}^- \rightarrow \frac{5}{2}^-$	585.1	100(4)	-0.10(2)	<0.31	<5.2	0.00003	0.879	9.17 -4.39
1500.0 <sup>IS</sup>	1170(300) <sup>†</sup>	$\frac{9}{2}^- \rightarrow \frac{5}{2}^-$	689.5(1)	18(3)	$E2$		$27_{-9}^{+15}$	-	10.63	35.39 -15.21
1572.1 <sup>IS</sup>	$280_{-100}^{+210}$	$\frac{3}{2}^- \rightarrow \frac{3}{2}^-$	885.1*	37(5)	-1.60(14)	0.02(1)	$36_{-19}^{+27}$	0.002	14.46	25.71 -8.85
		$\frac{5}{2}^- \rightarrow \frac{5}{2}^-$	761.4*	100(5)	-0.28(3)	$0.27_{-0.12}^{+0.16}$	$21_{-10}^{+12}$	0.00001	6.0	16.66 -6.44
		$\frac{5}{2}^- \rightarrow \frac{5}{2}^-$	287.4*	20(5)	(M1)	<1.09				
1588.4 <sup>IS*</sup>	> 1260	$\frac{5}{2}^- \rightarrow \frac{3}{2}^-$	901.2*	100(8)	-0.53(6)	<0.04	<8	0.0012	4.36	17.18 -5.26
		$\frac{5}{2}^- \rightarrow \frac{5}{2}^-$	777.8*	18(8)	$-4.03_{-3.45}^{+1.32}$	<0.001	<13	0.0069	16.94	34.19 -12.37
1779.7 <sup>IV</sup>	$105_{-28}^{+43}$	$\frac{5}{2}^- \rightarrow \frac{3}{2}^-$	1092.4*	8(5)	0.05(9)	$0.03_{-0.02}^{+0.04}$	$0.04_{-0.03}^{+0.04}$	0.037	0.306	-0.74 2.35
		$\frac{5}{2}^- \rightarrow \frac{5}{2}^-$	969.0	100(5)	0.04(6)	$0.55_{-0.18}^{+0.24}$	0.5(2)	0.616	0.0001	-0.72 4.92
		$\frac{1}{2}^- \rightarrow g.s.$						-	4.28	12.63 19.87
1840.6 <sup>IV*</sup>	$103_{-24}^{+35}$	$\frac{3}{2}^-, \frac{5}{2}^- \rightarrow \frac{3}{2}^-$	1153.4*	100(4)	0.14(4), 0.26(6)	0.29(8), 0.28(9)	2.5(7), 8(2)	0.462	0.306	-4.36 4.90
		$\frac{5}{2}^- \rightarrow \frac{5}{2}^-$	1029.6*	20(4)	0.32(6), 0.17(8)	0.08(3), 0.08(3)	4(1), 1(1)	0.046	0.078	-1.91 2.63
		$\frac{1}{2}^- \rightarrow g.s.$						-	5.99	13.03 14.55
1948.1	$230_{-69}^{+133}$	$\frac{7}{2}^- \rightarrow \frac{5}{2}^-$	1137.4	100	0.05(4)	0.17(7)	0.2(1)			
1997.6*	$92_{-17}^{+22}$	$\frac{5}{2}^- \rightarrow \frac{3}{2}^-$	1310.2*	12(5)	-0.29(12)	0.03(2)	$0.8_{-0.4}^{+0.6}$			
		$\frac{5}{2}^- \rightarrow \frac{5}{2}^-$	1186.9*	100(5)	-0.31(11)	$0.30_{-0.07}^{+0.09}$	$12_{-3}^{+4}$			
2012.6*		$\frac{3}{2}^- \rightarrow \frac{3}{2}^-$	1325.8*	100(5)	$4.47_{-0.94}^{+1.53}$					
		$\frac{3}{2}^- \rightarrow \frac{3}{2}^-$	440.4*	6(5)						
2024.4 <sup>IS*</sup>	$78_{-25}^{+41}$	$\frac{3}{2}^- \rightarrow \frac{3}{2}^-$	1337.1*	100(3)	$-4.70_{-1.28}^{+0.84}$	0.01(1)	$91_{-53}^{+76}$			
		$\frac{3}{2}^- \rightarrow \frac{3}{2}^-$	452.1*	3(3)	(M1)	< 0.23				
2099.6	$133_{-36}^{+62}$	$\frac{7}{2}^- \rightarrow \frac{5}{2}^-$	1288.9*	46(7)	-0.05(5)	0.05(1)	$0.2_{-0.1}^{+0.3}$			
		$\frac{7}{2}^- \rightarrow \frac{7}{2}^-$	703.8	100(7)						
2127.1*	$235_{-109}^{+171}$	$\frac{5}{2}^- \rightarrow \frac{5}{2}^-$	1383.1*	13(4)						
		$\frac{5}{2}^- \rightarrow \frac{5}{2}^-$	1316.61*	10(4)						
		$\frac{7}{2}^- \rightarrow \frac{7}{2}^-$	731.3*	18(4)						
		$\frac{7}{2}^- \rightarrow \frac{7}{2}^+$	626.9*	100(4)						
2153.8*	$115_{-20}^{+28}$	$\frac{1}{2}^- \rightarrow \frac{1}{2}^-$	2122.8*	100						

<sup>†</sup> Data taken from Ref. [38].

<sup>q</sup> Lifetime taken from Ref. [46].



These large  $B(E2)$  values support the  $IS$  character of the state. Decay to the ground state has not been observed. The strong  $E2$  transitions to the one-phonon states confirm the  $IS$  character.

#### 6. 1588.1 $5/2_{IS}^-$ state

A lower limit for the lifetime of  $>1260$  fs has been determined for this level, giving upper limits for the  $B(E2)$  values to the  $3/2^-$  and  $5/2^-$  one-phonon states of  $<8$  and  $<13$  W.u., respectively. Although the experimental data are not conclusive, our  $SM$  calculations predict relatively strong transitions and isoscalar character for the transitions to the one-phonon states, which support the  $IS$  character.

#### 7. 1779.7 keV $5/2_{IV}^-$ state

Although the identification of  $MS$  states have already been discussed in [8], we include them for completeness. The previously proposed ( $5/2^-$ ) level at 1779.7 keV yields a new 1092-keV branch to the first  $3/2_1^-$  excited state that has been revealed from the excitation function and coincidence data. The level has been assigned as  $J^\pi=5/2^{(-)}$  by the analysis of the angular correlation data, and a mean lifetime of  $105_{-28}^{+43}$  fs has been determined [8]. The 969 and 1092 keV transitions depopulating this state to the  $2p_{1/2}^{-1} \otimes 2^+$  symmetric one-phonon states provide branching ratios of 100(5) and 8(5), respectively, and mixing ratios,  $\delta$ , of 0.04(6) and 0.05(9), respectively. Hence, the 969 keV transition to the  $5/2_1^-$  state has a large  $B(M1)$  value of  $0.55_{-0.18}^{+0.24} \mu_N^2$  and a small  $B(E2)$  value of 0.5(2) W.u., while the 1092 keV transition to the  $3/2_1^-$  state exhibits a much weaker  $B(M1)$  strength of  $0.03_{-0.02}^{+0.04} \mu_N^2$  and a  $B(E2)$  value of  $0.04_{-0.03}^{+0.04}$  W.u. A large  $B(M1)$  value to the  $5/2^-$  one-phonon state was predicted, together with strong isovector character for such a transition.

#### 8. 1840.6 keV $3/2_{IV}^-$ state

The 1840.6 keV level has been placed from our measurements. The angular correlation analysis of the competing branches depopulating this state (see Table II) leads equally to either  $J^\pi=3/2^-$  or  $5/2^-$  assignments. A mean lifetime of  $103_{-24}^{+35}$  fs has been measured for this state, yielding large  $B(M1)$  values of 0.29(8)  $\mu_N^2$  ( $J^\pi=3/2^-$ ) or 0.28(9)  $\mu_N^2$  ( $J^\pi=5/2^-$ ) for the 1153 keV transition. We proposed, however, that this state is  $3/2^-$ , based on its proximity to the 1779.7 keV level and their rather different decay strengths. A large  $B(M1)$  value, this time to the  $3/2^-$  one-phonon state was predicted.

The  $B(M1)$  values from the 1779.7-keV state to the  $5/2_1^-$  level and from the proposed 1840.6 keV state to

the  $3/2_1^-$  level are greater than from any other negative-parity states feeding the symmetric one-phonon states. These observations, together with the appearance of these states in the expected energy range ( $\sim 2$  MeV), support their assignment as first-order isovector excitations.

The increasing level density and stronger mixing above 1.9 MeV make the attempt of characterization of other excitations unrewarding.

## IV. DISCUSSION

### A. Shell-Model Calculations

For the present work, we solve the model space Schrödinger equation  $PH_{eff}P\Psi = EP\Psi$ , where  $H_{eff} = H_0 + V_{eff}$  and  $V_{eff}$  is the  $SM$  effective interaction. To derive  $V_{eff}$  we use the model space folded-diagram methods detailed in Ref. [47], where we have the explicit expansion for the effective interaction:

$$V_{eff} = \hat{Q} - \hat{Q}' \int \hat{Q} + \hat{Q}' \int \hat{Q} \int \hat{Q} - \hat{Q}' \int \hat{Q} \int \hat{Q} \int \hat{Q} + \dots \quad (5)$$

In this series,  $\hat{Q}$  represents the irreducible vertex function, consisting of irreducible valence-linked diagrams, and the integral sign denotes a generalized folding operation. In the  $\hat{Q}$ -box we have included core polarization diagrammatic contributions up to second order, which has been shown to be a good approximation to a non-perturbative all-order summation in the absence of  $3N$  forces [48]. The intermediate particle and hole states are allowed two oscillator shells above and below the model space (which is discussed below). We sum the above series using the Lee-Suzuki iteration method [49].

Starting from any high-precision NN interaction  $V_{NN}$ , we can derive a resolution-dependent low-momentum interaction  $V_{low k}$ , which preserves all low-energy data below the chosen momentum cutoff [11]. For this work we have used the CD-Bonn interaction as  $V_{NN}$  with a momentum cutoff value of  $\Lambda = 2.0 \text{ fm}^{-1}$ . There have now been a number of nuclear structure studies using this low-momentum NN interaction in this nuclear region to describe a variety of nuclei and their observables [8, 50–52].

Following the prescription of Ref. [10], we choose to use  $^{88}\text{Sr}$  as the inert core for these calculations. Valence neutrons can then occupy the following single-particle orbits above the  $N = 50$  closed shell:  $g_{7/2}$ ,  $d_{5/2}$ ,  $d_{3/2}$ ,  $s_{1/2}$ , and  $h_{11/2}$ . For the valence protons, we take the  $p_{1/2}$  and  $g_{9/2}$  orbits consistent with a  $Z = 38$  proton core. The single-particle energies,  $\epsilon_j$ , were obtained from the experimental values in the  $^{89}\text{Y}$  and  $^{89}\text{Sr}$  nuclei; for reference, they are listed in Table III. These single-particle energies differ slightly from those used in Ref. [8], which were tuned to

TABLE III. Single-particle energies for the orbits used in *SM* calculations.

Proton orbits:	$p_{1/2}$	$g_{9/2}$			
Energy (MeV)	-0.91	0.0			
Neutron orbits:	$g_{7/2}$	$d_{5/2}$	$d_{3/2}$	$s_{1/2}$	$h_{11/2}$
Energy (MeV)	1.47	0.0	2.01	1.03	3.00

best reproduce the experimental spectra in  $^{90}\text{Zr}$  and  $^{90}\text{Sr}$ . To keep the calculations as free from adjustable parameters as possible, we now use the experimental values, but our current results on the negative-parity states in  $^{93}\text{Nb}$  are essentially unchanged from those reported earlier [8].

To test this interaction, we have compared the calculated proton-proton (*pp*) and neutron-neutron (*nn*) spectra with the experimentally observed spectra for the  $^{90}\text{Sr}$  and  $^{90}\text{Zr}$  nuclei up to excitation energies of  $\sim 3$  MeV [53]. Here, we see there is generally fair agreement between the calculated and experimental levels, noting that the  $V_{\text{low } k}$  calculation gave rather similar results to the those obtained in Ref. [10], in which the surface delta interaction, with tuned parameters, was used as the residual interaction. Particularly, Figure 4 shows a partial level scheme with first-order *IS* and *IV* positive-parity excitations identified in this work compared with  $V_{\text{low } k}$  *SM* calculations. The calculations were carried out using the OXBASH *SM* code [54] with a model space file and  $V_{\text{low } k}$  interaction file specifically generated, using the above single-particle energies, for use with this code.

For comparison with experimental work, we explicitly calculate the transition rates, defined as:

$$B(M1 : J_i \rightarrow J_f) = \frac{|\langle J_f || M1 || J_i \rangle|^2}{2J_i + 1}. \quad (6)$$

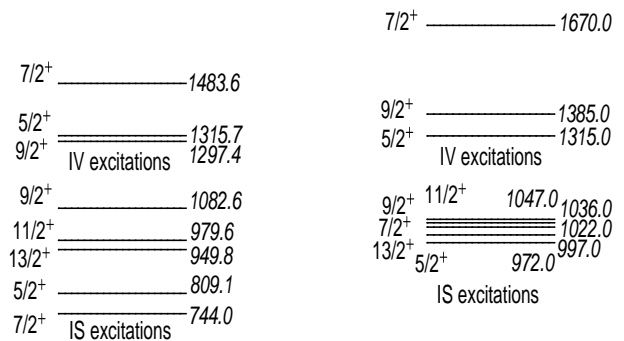
In these calculations we have kept the bare orbital *g*-factors,  $g_\pi^l = 1\mu_N$  and  $g_\nu^l = 0$ , while we have used empirical values for the spin *g*-factors,  $g_\pi^s = 3.18\mu_N$  and  $g_\nu^s = -2.18\mu_N$ . We note that these values for the spin *g* factors are not fit to any experimental data. Similarly, the *E2* transition operator is given by

$$T(E2) = e_\pi \sum_{i=1}^Z r_i^2 Y_\mu^{(2)}(\hat{r}_i) + e_\nu \sum_{i=1}^N r_i^2 Y_\mu^{(2)}(\hat{r}_i), \quad (7)$$

where  $e_\pi$  and  $e_\nu$  are the proton and neutron effective charges. Here, we use the same effective charges as in Ref. [8]; that is,  $e_\pi = 1.85e$  and  $e_\nu = 1.30e$ .

## B. Positive-Parity States

In even-even nuclei the signature of large magnetic dipole transition strength from a proposed isovector excitation to the isoscalar state is typically sufficient for



9/2+ 0.0 Experiment  $V_{\text{low } k}$  SM calculations 9/2+ 0.0

FIG. 4.  $^{93}\text{Nb}$  partial level scheme showing first-order *IS* and *IV* positive-parity excitations (left) as compared with  $V_{\text{low } k}$  *SM* calculations (right).

identification of *MS* states. Due to the presence of an unpaired nucleon in an odd-mass nucleus, however, further theoretical evidence is needed to confidently identify a *MS* state. Here, in addition to the magnetic dipole transition rates, we decompose the relevant transitions into their spin and orbital components to rule out large *M1* strengths due to spin-flip transitions. The calculations are presented in Table IV, where we have only included the results for states where a clearly analogous state was experimentally present.

### 1. First-order *IS* excitations

The lowest-lying quintet  $\{5/2_1^+, 7/2_1^+, 9/2_2^+, 11/2_2^+, 13/2_2^+\}$  can clearly be identified as the coupling of the  $g_{9/2}$  proton to the  $2_1^+$  state in  $^{92}\text{Zr}$ . While the experiments were not sensitive to the ground-state decay rates of these states, the *SM* calculations reveal all to have strongly collective *B(E2)* transition rates to the  $9/2^+$  ground state, with predominantly isoscalar character.

### 2. First-order *IV* excitations

We start with the 1279.4 keV  $9/2^+$  state, which exhibits a strong *M1* transition to the symmetric one-phonon  $7/2_1^+$  state and a weakly collective *E2* transition to the  $9/2^+$  ground state experimentally. In the calculations, we find a qualitatively similar decay pattern, though the rates are slightly underpredicted in the *SM* calculations. In Table IV, we see that this magnetic

TABLE IV. Spin and orbital contributions to the large  $M1$  transitions observed in the SM calculations. Values are given in units of  $\mu_N^2$ .

$J_i$	$\rightarrow J_f$	Spin $B(M1)$	Orbital $B(M1)$
$5/2_2^+$	$\rightarrow 7/2_1^+$	0.1434	0.1280
$7/2_3^+$	$\rightarrow 9/2_1^+$	0.1248	0.09257
	$\rightarrow 5/2_1^+$	0.05369	0.04515
$9/2_3^+$	$\rightarrow 7/2_1^+$	0.05797	0.06953
$11/2_2^+$	$\rightarrow 13/2_1^+$	0.03941	0.03586

dipole transition is almost equally composed of spin and orbital parts, as is typically seen in such transitions [8], leading to a confident assignment as a MS excitation.

The 1483 keV  $7/2^+$  state exhibits a similar experimental decay pattern, with strong  $M1$  transitions to both the  $9/2_1^+$  and  $5/2_1^+$  states (though only an upper bound is determined for the transition to the  $9/2_1^+$  state) and a weakly  $E2$  transition to the ground state. In the SM calculations the large  $M1$  transitions are again in qualitative agreement with the experimental measurements. In the calculations the transition to the ground state, however, is significantly more collective than the experimental value, but not inconsistent with its proposed identification as a MS excitation. To confirm this, we again turn to Table IV, where we see that for both of these  $M1$  transitions there is significant orbital character, indicating a MS state.

From an inspection of  $M1$  transition strength, it appears that the 1315 keV  $5/2^+$  state would be a reasonable  $IV$  excitation candidate with a strong transition to the  $7/2_1^+$  state. This is coupled with a collective  $E2$  transition to the same state, indicative of an  $IS$  transition. This is perhaps due to mixing between this and the 1665.6-keV  $5/2^+$  state, which also exhibits a weaker but sizable  $M1$  transition to the  $7/2_1^+$  state as well as a collective  $E2$  transition to the same state. The SM presents a picture consistent with this assessment, predicting an additional magnetic dipole transition to the  $5/2_1^+$  state not seen experimentally. The MS character

of these large  $M1$  transitions can be confirmed in Table IV, where we see a sizable orbital component of the transitions.

Finally, a case can be made for proposing the 1603-keV  $11/2^+$  state as a member of the  $IV$  quintet due to the experimentally observed  $M1$  transition to the  $13/2_1^+$  one-phonon symmetric state. This is borne out in the calculations, where we see the expected equal distribution of spin and orbital  $M1$  transition strength. Again, some mixing with higher  $IS$  excitations is likely manifested in the collective  $E2$  transition to the one-phonon symmetric states seen experimentally, which are also apparent in the SM.

It would seem that a suitable candidate for the  $13/2^+$   $IV$  excitation is the 1686 keV state, with a large  $M1$  to both the  $11/2_1^+$  and  $13/2_1^+$  states observed experimentally. This, however, is unfortunately not apparent in the SM calculations as the  $M1$  transitions predicted are too weak to support this identification.

## V. CONCLUSION

In this work, we have investigated  $IV$  and  $IS$  excitations in the positive- and negative-parity structures of  $^{93}\text{Nb}$ . Identifications are based on from  $M1$  and  $E2$  transition strengths, spin and parity assignments, and shell model calculations. These findings support the weak-coupling picture of fermions and bosons in both  $\pi 2p_{1/2}^{-1} \otimes ^{94}\text{Mo}$  and  $\pi 1g_{9/2} \otimes ^{92}\text{Zr}$  configurations. The marked separation of the positive- and negative-parity structures in  $^{93}\text{Nb}$  facilitates the comprehension of such a relevant interaction, specially in the simpler scenario for the negative-parity states. Overall, larger  $B(M1)$  values are observed in this nucleus as compared with the even- $A$  neighbors as the result of additional spin-flip effects. Levels assigned as  $IV$  excitations lie at lower energies than that observed for the  $2_{1,MS}^+$  state in  $^{92}\text{Zr}$  (1.847 MeV). Interestingly, similar transition strengths of about 30 W.u. are found from the levels characterised as  $IS$  excitations.

This work was supported by the U.S. National Science Foundation under Grant No. PHY-0652415, the Deutsche Forschungsgemeinschaft, Grant No. Jo 391/3-1 and by the U.S. Department of Energy under DE-FC02-07ER41457 (UNEDF SciDAC Collaboration). TRIUMF receives federal funding via a contribution agreement through the National Research Council of Canada.

[1] N. Lo Iudice and F. Palumbo, Phys. Rev. Lett. **41**, 1532 (1978).  
 [2] I. Bauske, J.M. Arias, P. von Brentano, A. Frank, H. Friedrichs, R.D. Heil, R.-D. Herzberg, F. Hoyler, P. Van Isacker, U. Kneissl, J. Margraf, H.H. Pitz, C. Wesselborg, and A. Zilges, Phys. Rev. Lett. **71**, 975 (1993).  
 [3] A. Nord, A. Schiller, T. Eckert, O. Beck, J. Besserer, P. von Brentano, R. Fischer, R.-D. Herzberg, D. Jager, U.

Kneissl, J. Margraf, H. Maser, N. Pietralla, H.H. Pitz, M. Rittner, and A. Zilges, Phys. Rev. C **54**, 2287 (1996).  
 [4] A. Nord, J. Enders, A.E. de Almeida Pinto, D. Belic, P. von Brentano, C. Fransen, U. Kneissl, C. Kohstall, A. Linnemann, P. von Neumann-Cosel, N. Pietralla, H.H. Pitz, A. Richter, F. Stedile, and V. Werner, Phys. Rev. C **67**, 034307 (2003).  
 [5] N. Huxel, P. von Brentano, J. Eberth, J. Enders, R.-

- D. Herzberg, P. von Neumann-Cosel, N. Nicolay, N. Pietralla, H. Prade, C. Rangacharyulu, J. Reif, A. Richter, C. Schlegel, R. Schwengner, S. Skoda, H.G. Thomas, I. Wiedenhöver, G. Winter, and A. Zilges, Nucl. Phys. A **645**, 239 (1999).
- [6] N. Pietralla, P. von Brentano, and A.F. Lisetskiy, Prog. Part. Nucl. Phys. **60**, 225 (2008).
- [7] F. Iachello and A. Arima, Interacting Boson Model, Oxford University Press, 1990.
- [8] J. N. Orce, J. D. Holt, A. Linnemann, C. J. McKay, S. R. Leshner, C. Fransen, J. W. Holt, A. Kumar, N. Warr, V. Werner, J. Jolie, T. T. S. Kuo, M. T. McEllistrem, N. Pietralla, and S. W. Yates, Phys. Rev. Lett. **97**, 062504 (2006).
- [9] B. Cheal, K. Baczyńska, J. Billowes, P. Campbell, F.C. Charlwood, T. Eronen, D. H. Forest, A. Jokinen, T. Kessler, I. D. Moore, M. Reponen, S. Rothe, M. Ruffer, A. Saastamoinen, G. Tungate, and J. Aysto, Phys. Rev. Lett. **102**, 222501 (2009).
- [10] A.F. Lisetskiy, N. Pietralla, C. Fransen, R.V. Jolos, and P. von Brentano, Nucl. Phys. A **677**, 100 (2000).
- [11] S. K. Bogner, T. T. S. Kuo, and A. Schwenk, Phys. Rep. **386**, 1 (2003).
- [12] M. T. McEllistrem, *Nuclear Research with Low Energy Accelerators*, Academic Press, New York (1967), p. 167; P.E. Garrett, N. Warr, and S.W. Yates, J. Res. Natl. Inst. Stand. Technol. **105**, 141 (2000).
- [13] T. Belgya, G. Molnár, and S.W. Yates, Nucl. Phys. A **607**, 43 (1996).
- [14] A.E. Blaugrund, Nucl. Phys. **88**, 501 (1966).
- [15] K. B. Winterbon, Nucl. Phys. A **246**, 293 (1975).
- [16] C.A. McGrath, P.E. Garrett, M.F. Villani, and S.W. Yates, Nucl. Instr. Meth. A **421**, 458 (1999).
- [17] A. Linnemann, PhD thesis, IKP, University of Cologne (2005).
- [18] J. Eberth, H. G. Thomas, P. von Brentano, R. M. Lieder, H.M. Jäger, H. Kämmerfing, M. Berst, D. Gutknecht, and R. Henck, Nucl. Instr. Meth. A **369**, 135 (1996).
- [19] H.J. Rose and B.M. Brink, Rev. Mod. Phys. **39** 306 (1967).
- [20] K.S. Krane and R.M. Steffen, Phys. Rev. C **2**, 724 (1970); K.S. Krane, R.M. Steffen, and R.M. Wheeler, Nucl. Data Tab. **11**, 351 (1973).
- [21] I. J. van Heerden and W. R. McMurray, Z. Physik **260**, 9 (1973).
- [22] T. Kakavand and K. P. Singh, Acta Phys. Pol. B **33**, 737 (2002).
- [23] <http://www.nndc.bnl.gov>. (*NNDC database*)
- [24] H. C. Sharma and N. Nath, Nucl. Phys. A **142**, 291 (1970).
- [25] H. Göbel, E. J. Feicht and H. Vonach, Z. Physik **240**, 430 (1970).
- [26] M. R. Cates, J. B. Ball and E. Newman, Phys. Rev. **187**, 1682 (1969).
- [27] K. Heyde and P. J. Brussaard, Nucl. Phys. A **104**, 81 (1967).
- [28] A. Bohr and B. R. Mottelson, Mat. Fys. Medd. Dan. Vid. Selsk. **27**, No.16 (1953).
- [29] D. C. Choudhury, Mat. Fys. Medd. Dan. Vid. Selsk. **28**, No.4 (1954).
- [30] R. D. Lawson and J. L. Uretsky, Phys. Rev. **108**, 1300 (1957).
- [31] A. de-Shalit, Phys. Rev. **122**, 1530 (1961).
- [32] R. E. Anderson, J. J. Kraushaar, I. C. Oelrich, R. M. DelVecchio, R. A. Naumann, E. R. Flynn, and C. E. Moss, Phys. Rev. C **15**, 123 (1977).
- [33] I. C. Oelrich, K. Krien, R. M. DelVecchio, and R. A. Naumann, Phys. Rev. C **14**, 563 (1976).
- [34] C. Fransen, V. Werner, D. Bandyopadhyay, N. Boukharouba, S.R. Leshner, M.T. McEllistrem, J. Jolie, N. Pietralla, P. von Brentano, and S.W. Yates, Phys. Rev. C **71**, 054304 (2005).
- [35] M. E. Bunker, B. J. Dropesky, J. D. Knight, and J. W. Starnes, Phys. Rev. **127**, 844 (1962).
- [36] Y. Yoshizawa, B. Herskind, and M. Hoshi, J. Phys. Soc. Jap. **50**, 2151 (1981).
- [37] M. Kregar and G. G. Seaman, Nucl. Phys. A **179**, 153 (1972).
- [38] P.H. Stelson, R.L. Robinson, W.T. Milner, F.K. McGowan, and M.A. Ludington, Bull. Am. Phys. Soc. **16**, 619 (1971).
- [39] K. Alder, A. Bohr, T. Huus, B. Mottelson, and A. Winther, Rev. Mod. Phys. **28**, 432 (1956).
- [40] J.J. Kent, W.R. Coker, and C.E. Watson, Z. Phys. **256**, 199 (1972).
- [41] C. Fransen, N. Pietralla, Z. Ammar, D. Bandyopadhyay, N. Boukharouba, P. von Brentano, A. Dewald, J. Gableske, A. Gade, J. Jolie, U. Kneissl, S.R. Leshner, A.F. Lisetskiy, M.T. McEllistrem, M. Merrick, H.H. Pitz, N. Warr, V. Werner, and S.W. Yates, Phys. Rev. C **67**, 024307 (2003).
- [42] V. Werner, D. Belic, P. von Brentano, C. Fransen, A. Gade, H. von Garrel, J. Jolie, U. Kneissl, C. Kohstall, A. Linnemann, A.F. Lisetskiy, N. Pietralla, H.H. Pitz, M. Scheck, K.-H. Speidel, F. Stedile, and S.W. Yates, Phys. Lett. B **550**, 140 (2002).
- [43] I.K. Lemberg and A.A. Pasternak, Izv. Akad. Nauk SSSR, Ser.Fiz. **38**, 1600 (1974).
- [44] V. D. Avchukhov, K. A. Baskova, V. A. Bondarenko, A. B. Vovk, L. I. Govor, and A. D. Demidov, Izv. Akad. Nauk SSSR, Ser. Fiz. **46**, 947 (1982).
- [45] J. Enders, N. Huxel, P. von Neumann-Cosel, and A. Richter, Phys. Rev. Lett. **79**, 2010 (1997).
- [46] C. M. Baglin, Nuclear Data Sheets **80**, 1 (1997).
- [47] T. T. S. Kuo and E. Osnes, *Lecture Notes in Physics* (Springer-Verlag, New York, 1990), Vol. 364.
- [48] J. D. Holt, J. W. Holt, T. T. S. Kuo, G. E. Brown, and S. K. Bogner, Phys. Rev. C **72**, 041304(R) (2005).
- [49] K. Suzuki and S. Y. Lee, Prog. Theor. Phys. **64**, 2091 (1980).
- [50] J. D. Holt, N. Pietralla, J. W. Holt, T. T. S. Kuo, and G. Rainovski, Phys. Rev. C **76**, 034325 (2007).
- [51] O. Burda, N. Botha, J. Carter, R. W. Fearick, S. V. Förtsch, C. Fransen, H. Fujita, J. D. Holt, M. Kuhar, A. Lenhardt, P. von Neumann-Cosel, R. Neveling, N. Pietralla, V. Yu. Ponomarev, A. Richter, O. Scholten, E. Sideras-Haddad, F. D. Smit, and J. Wambach, Phys. Rev. Lett. **99**, 092503 (2007).
- [52] V. Werner, N. Benczer-Koller, G. Kumbartzki, J. D. Holt, P. Boutachkov, E. Stefanova, M. Perry, N. Pietralla, H. Ai, K. Aleksandrova, G. Anderson, R. B. Cakirli, R. J. Casperson, R. F. Casten, M. Chamberlain, C. Cocos, B. Darakchieva, S. Eckel, M. Evtimova, C. R. Fitzpatrick, A. B. Garnsworthy, G. Gurdal, A. Heinz, D. Kovacheva, C. Lambie-Hanson, X. Liang, P. Manchev, E. A. McCutchan, D. A. Meyer, J. Qian, A. Schmidt, N. J. Thompson, E. Williams, R. Winkler, Phys. Rev. C **78**, 031301(R) (2008).

- [53] J. D. Holt, N. Pietralla, J. W. Holt, and T. T. S. Kuo, in preparation.
- [54] B. A. Brown, A. Etchegoyen, N. S. Godwin, W. D. M. Rae, W. A. Richter, W. E. Ormand, E. K. Warburton, J. S. Winfield, L. Zhao, and C. H. Zimmerman, MSU-NSCL report number 1289.